Konstantin Meskouris
Christoph Butenweg · Klaus-G. Hinzen
Rüdiger Höffer

Structural Dynamics with Applications in Earthquake and Wind Engineering

Second Edition

Springer

Structural Dynamics with Applications in Earthquake and Wind Engineering

Konstantin Meskouris · Christoph Butenweg
Klaus-G. Hinzen · Rüdiger Höffer

Structural Dynamics with Applications in Earthquake and Wind Engineering

Second Edition

With contributions from Ana Cvetkovic, Linda Giresini, Britta Holtschoppen, Francesca Lupi, Hans-Jürgen Niemann

Springer

Konstantin Meskouris
Lehrstuhl für Baustatik und Baudynamik
RWTH Aachen University
Aachen, Germany

Christoph Butenweg
FH Aachen—University
of Applied Sciences
Aachen, Germany

Klaus-G. Hinzen
Erdbebenstation Bensberg, Institut
für Geologie und Mineralogie
Universität zu Köln
Bergisch Gladbach, Nordrhein-Westfalen
Germany

Rüdiger Höffer
Fakultät für Bau- und
Umweltingenieurwissenschaften
Ruhr-Universität Bochum
Bochum, Nordrhein-Westfalen
Germany

ISBN 978-3-662-57548-2 ISBN 978-3-662-57550-5 (eBook)
https://doi.org/10.1007/978-3-662-57550-5

Library of Congress Control Number: 2018949059

Originally published by Ernst & Sohn Verlag, Berlin, 2000

This Springer imprint is published by the registered company Springer-Verlag GmbH, DE part of Springer Nature.
The registered company address is: Heidelberger Platz 3, 14197 Berlin, Germany

Preface

The traditional design philosophy for buildings and structures, which takes almost exclusively only statics considerations into account, is being steadily supplemented by the need for carrying out additional verifications concerning their response and safety under dynamic loads. A reason for this may lie in the proliferation of modern bold architectural design forms favouring unorthodox and/or very slender structures, which are often susceptible to vibration under dynamic excitation. In addition, satisfying higher safety demands is increasingly required for buildings serving important societal needs (e.g. hospitals), or structures with high intrinsic risk potential (e.g. large industrial units). A prerequisite for carrying out complex dynamic analyses is a familiarity with the theoretical foundations and numerical methods of structural dynamics together with experience in the application of the latter and an insight into the nature of dynamic loads. The present book addresses both students and practising civil engineers offering an overview of the theoretical basics of structural dynamics complete with the relevant software for analysing the response of structures subject to earthquake and wind loads and illustrating its use by means of many examples worked out in detail, with input files for the programmes included. In the spirit of "learning by doing", it thus encourages readers to apply the tools described to their own problems, allowing them to become familiar with the broad field of structural dynamics in the process. Chapter 1 deals with the basic theory of structural dynamics followed by chapters on wind and earthquake loads. Chapters 4 and 5 deal with the behaviour of buildings and industrial units under seismic loading, respectively, while the final chapter is devoted to the application of wind engineering methods to slender tower-like structures. May this book contribute to a deeper understanding and familiarity of civil engineering students and practising engineers with the standard structural dynamics methods, enabling them to confidently carry out all necessary calculations for evaluating and verifying the safety of buildings and structures!

Aachen, Germany — Konstantin Meskouris
Aachen, Germany — Christoph Butenweg
Bergisch Gladbach, Germany — Klaus-G. Hinzen
Bochum, Germany — Rüdiger Höffer

Contents

Authors and Contributors

About the Authors

Prof. Dr.-Ing. Konstantin Meskouris was born in Athens, Greece. He studied Civil Engineering in Vienna and Munich, graduating in 1970 at the Technical University (TU) Munich, from which he also received his doctoral degree. From 1996 until his retirement in 2012, he served as Head of the Institute for Structural Statics and Dynamics in the Civil Engineering Department of RWTH Aachen University.

Prof. Dr.-Ing. Christoph Butenweg was born in Borken, Germany. He graduated in Civil Engineering at the Ruhr-Universität Bochum. From 1994 to 1999, he served as Research Assistant at Essen University and subsequently as Senior Engineer at the Institute of Structural Statics and Dynamics of RWTH Aachen University. Since 2006, he has been Manager of the SDA-engineering GmbH in Herzogenrath and since 2016 Full Professor for Technical Mechanics and Structural Engineering at FH Aachen—University of Applied Sciences.

Prof. Dr. Klaus-G. Hinzen was born in Hagen, Germany. He studied Geophysics at the Ruhr-Universität Bochum, graduating in 1979 and receiving his doctorate there in 1984. From 1984 to 1995, he served as Researcher at the Federal Institute for Geosciences and Natural Resources, Hanover. Since 1995, he has been Head of the Seismological Station Bensberg of Cologne University.

Prof. Dr.-Ing. Rüdiger Höffer was born in Attendorn, Germany. He graduated in Civil Engineering at Ruhr-Universität Bochum where he afterwards served as a research assistant. In 1996, he earned his doctoral degree in Bochum and subsequently spent two years as a postdocoral researcher abroad. He gained practical experience as a project engineer and managing director of consulting offices at Düsseldorf and Bochum, Germany. In 2003, he was appointed Full Professor for Wind Engineering at the Ruhr-Universität Bochum.

Contributors

Ana Cvetkovic M.Sc., born at Pozarevac, Serbia, earned her bachelor diploma in Structural Engineering at Belgrade University and graduated master's degree in Computational Engineering at the Ruhr-Universität Bochum in 2017. Since 2017, she works as Project Engineer in structural engineering.

Linda Giresini was born in Tempio, Italy. She earned her doctoral degree in Civil Engineering at the University of Pisa. She worked as Researcher at the Institute of Structural Statics and Dynamics, RWTH Aachen University and at the Institute for Sustainability and Innovation in Structural Engineering, University of Minho (Portugal) in 2013–2014. From 2014 to 2015, she was Research Assistant at the University of Sassari, Italy. Since 2016, she has been working as Assistant Professor of Structural Design at the University of Pisa.

Dr.-Ing. Britta Holtschoppen studied Civil Engineering at RWTH Aachen University and graduated in 2004. After a research stay at the University of Bristol, Great Britain, she returned to the Chair of Structural Statics and Dynamics of RWTH Aachen University and focused her research on the seismic design of industrial facilities with special emphasis on secondary structures, tank structures and probabilistic seismic performance assessment. Since 2016, she has worked at SDA-engineering GmbH, Herzogenrath.

Dr.-Ing. Francesca Lupi was born in Prato, Italy. She graduated master's degree in Civil Engineering at the Universita Degli Studi di Firenze, Italy, and earned her doctoral degree in 2013 in a joint programme of her home university and the Technische Universität Braunschweig. In 2015, she received a research scholarship for postdocs from the Alexander-von-Humboldt Foundation, Germany. Since 2018, she is employed as Senior Research Assistant at the Ruhr-Universität Bochum.

Prof. Dr.-Ing. habil. Hans-Jürgen Niemann was born 1935 in Lüneburg, Germany. He studied Civil Engineering at the Universität Hannover and graduated as Diplomingenieur. He worked as Research Assistant at the Universität Hannover and the then newly established Ruhr-Universität Bochum, graduated as Doctor of Civil Engineering and obtained the habilitation in Structural Engineering from the Ruhr-Universität Bochum. He was appointed Full Professor of Wind Engineering and Fluid Mechanics and served at the Department of Civil Engineering at Ruhr-Universität Bochum until 2001. In the same year, he founded the Engineering Company Niemann und Partners, Bochum.

Chapter 1
Basic Theory and Numerical Tools

Konstantin Meskouris

Abstract This chapter offers an overview of the theoretical foundations and the standard numerical methods for solving structural dynamics problems, with emphasis placed firmly on the latter. Starting with the analysis of single degree of freedom (SDOF) systems both in the time and in the frequency domain, it includes sections on the computation of elastic and inelastic response spectra, filtering in the frequency domain, the analysis of nonlinear SDOF systems and the generation of spectrum compatible ground motion time histories. Discrete multi-degree of freedom (MDOF) systems, condensation techniques and damping models are considered next. Both modal analysis ("response modal analysis") and direct integration methods are employed, focussing especially on the behaviour of MDOF systems subject to seismic excitations described by response spectra or sets of specific ground motion time histories. Detailed descriptions of the software used for solving the numerous examples presented complete with full input-output parameter lists conclude the chapter.

Keywords SDOF system · Seismic excitation · Response spectrum
Spectrum compatible accelerogram · Damping · MDOF system · Modal analysis
Direct integration

In this section, the most important basics of structural dynamics are introduced, which are needed in the further chapters of this book. The explanation of the theoretical derivation is kept to a minimum, while the emphasis is set on practical applications. For most algorithms, easy to use computing programs are provided, which application is illustrated by several examples.

Electronic supplementary material The online version of this chapter (https://doi.org/10.1007/978-3-662-57550-5_1) contains supplementary material, which is available to authorized users.

K. Meskouris et al., *Structural Dynamics with Applications in Earthquake and Wind Engineering*, https://doi.org/10.1007/978-3-662-57550-5_1

1.1 Single-Degree-of-Freedom Systems

Single-degree-of-freedom (SDOF) systems are the simplest oscillators. In spite of their simplicity, they are being successfully used as numerical models in many real-life cases. They are discussed in some detail in this chapter because of their wide application range and also because due to their "straightforwardness" they are eminently suitable for introducing basic structural dynamics methods and concepts.

1.1.1 Linear SDOF Systems in the Time Domain

Figure 1.1 depicts the standard case of a viscously damped SDOF system subject to a time-varying external load F(t). From the free-body diagram we obtain by D'ALEMBERT'S principle

$$\underline{F}_I + \underline{F}_D + \underline{F}_R = \underline{F}(t) \tag{1.1.1}$$

with $\underline{F}_I$, $\underline{F}_D$ and $\underline{F}_R$ as inertia, damping and restoring force, respectively. Setting the inertia force equal to mass times acceleration, the damping force equal to a coefficient c times velocity (linear viscous damping model) and the restoring force equal to displacement times the spring stiffness k yields the following 2nd order inhomogeneous linear ordinary differential equation (ODE) with constant coefficients:

$$m \cdot \underline{\ddot{u}} + c \cdot \underline{\dot{u}} + k \cdot \underline{u} = \underline{F}(t) \tag{1.1.2}$$

In order to avoid numerical errors in practice, it is advisable to use a consistent system of units, in which mass/force conversions are taken care of automatically. This is e.g. the case when masses are expressed in tons (1 ton = 1000 kg), forces in kN, lengths in m and time in s. Accordingly, c in (1.1.2) might be given in units of kN s/m, k in kN/m, F in kN and u in m.

The general solution of (1.1.2) is equal to the sum of the solution of the homogeneous equation ($\underline{F}(t) = 0$) and a "particular integral". The homogeneous ODE

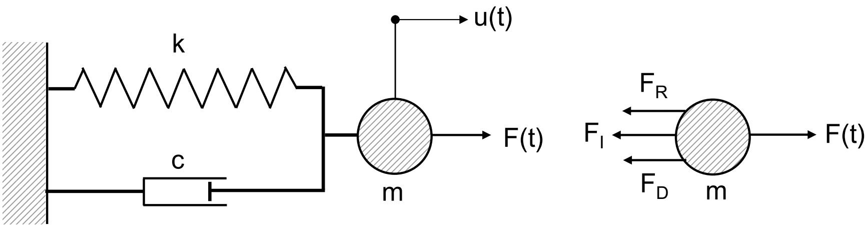

Fig. 1.1 SDOF system with free-body diagram

$$\underline{\ddot{u}} + \frac{c}{m} \cdot \underline{\dot{u}} + \frac{k}{m} \cdot \underline{u} = 0 \tag{1.1.3}$$

is satisfied by the function

$$u = e^{\lambda t};\ \dot{u} = \lambda\, e^{\lambda t};\ \ddot{u} = \lambda^2 e^{\lambda t} \tag{1.1.4}$$

leading to the characteristic equation

$$\lambda^2 + \frac{c}{m}\lambda + \omega_1^2 = 0; \quad \omega_1^2 = \frac{k}{m} \tag{1.1.5}$$

with ω_1 as circular natural frequency of the system. Its solutions are given by

$$\lambda_{1,2} = -\frac{c}{2m} \pm \sqrt{\left(\frac{c}{2m}\right)^2 - \omega_1^2} \tag{1.1.6}$$

The behaviour of the solution of the ODE depends on whether the radicand in Eq. (1.1.6) is less than, equal to or greater than zero, corresponding to the underdamped, critically damped and overdamped case, respectively. In the latter case, λ_1 and λ_2 are real and no vibration occurs. The critical damping is defined as the value of c for which the radicand is equal to zero:

$$\frac{c}{2m} = \omega_1 \rightarrow c_{krit} = 2m\,\omega_1 = 2\sqrt{km} \tag{1.1.7}$$

The dimensionless ratio D or ξ of the actual damping coefficient, c, to the critical damping, c_{krit}, called "damping ratio", is regularly used for quantifying damping. The following expressions hold:

$$D = \xi = \frac{c}{c_{krit}} = \frac{c}{2m\omega_1}; \frac{c}{m} = 2\xi\omega_1 \tag{1.1.8}$$

Table 1.1 summarizes some typical values for the damping ratio for low-amplitude building vibrations.

Introducing the damping ratio ξ and the natural circular frequency ω_1, the differential equation (1.1.3) can also be written as:

$$\ddot{u} + 2\xi\omega_1\dot{u} + \omega_1^2 u = 0 \tag{1.1.9}$$

Table 1.1 Damping ratios for different structural types

Type of structure	Damping ratio D or ξ (%)
Steel structure, welded	0.2–0.3
Steel structure, bolted	0.5–0.6
Reinforced concrete	1.0–1.5
Masonry	1.5–2

Its solution is

$$u(t) = e^{-\xi\omega_1 t}\left(C_1 \cos\sqrt{1-\xi^2}\omega_1 t + C_2 \sin\sqrt{1-\xi^2}\omega_1 t\right) \tag{1.1.10}$$

where C_1, C_2 are integration constants. For general initial conditions $u(0) = u_0, \dot{u}(0) = \dot{u}_0$ this leads to

$$u(t) = e^{-\xi\omega_1 t}(u_0 \cos\sqrt{1-\xi^2}\omega_1 t + \frac{(\dot{u}_0 + \xi\omega_1 u_0)}{\omega_1\sqrt{1-\xi^2}} \sin\sqrt{1-\xi^2}\omega_1 t) \tag{1.1.11}$$

This expression can be further simplified by introducing the damped natural circular frequency ω_D (corresponding damped natural period T_D):

$$\omega_D = \omega_1\sqrt{1-\xi^2}; \quad T_D = 2\pi/\omega_D \tag{1.1.12}$$

In the case of forced vibrations, Eq. (1.1.9) reads

$$\ddot{u} + 2\xi\omega_1\dot{u} + \omega_1^2 u = \frac{F(t)}{m} = f(t) \tag{1.1.13}$$

The general solution of (1.1.13) is given by the sum of the homogeneous solution Eq. (1.1.11) and the particular integral (DUHAMEL integral)

$$u_p(t) = \frac{1}{\omega_D}\int_0^t f(\tau)e^{-\xi\omega_1(t-\tau)} \sin\omega_D(t-\tau)d\tau \tag{1.1.14}$$

The DUHAMEL integral can be evaluated numerically for arbitrary forcing functions F(t). Alternatively, Eq. (1.1.13) can be solved by various Direct Integration algorithms as explained later.

Another widely used damping parameter, in addition to the critical damping ratio D or ξ according to Eq. (1.1.8), is the so-called logarithmic decrement Λ. It is defined as the natural logarithm of the ratio of the amplitudes of two successive positive (or negative) peaks:

$$\begin{aligned}\Lambda &= \ln\frac{u_i}{u_{i+1}} = \ln\frac{e^{-\xi\omega_1 t_i}\cos\omega_D t_i}{e^{-\xi\omega_1 t_{i+1}}\cos\omega_D t_{i+1}} = \ln e^{-\xi\omega_1(t_i - t_{i+1})} = \xi\omega_1(t_{i+1} - t_i)\\ &= \xi\omega_1\frac{2\pi}{\omega_D} = \xi\,\omega_1 T_D = \xi\,\omega_1\frac{2\pi}{\omega_1\sqrt{1-\xi^2}} = \xi\frac{2\pi}{\sqrt{1-\xi^2}}\end{aligned} \tag{1.1.15}$$

For the lightly damped systems normally encountered in structural dynamics, it is sufficiently accurate to write

$$\xi = D \approx \frac{\Lambda}{2\pi} \tag{1.1.16}$$

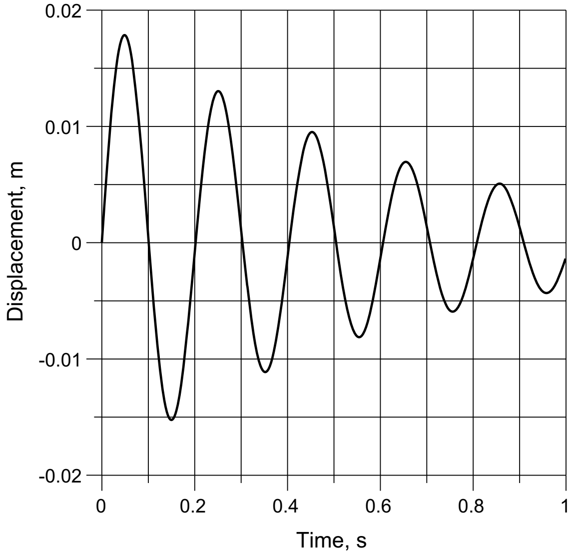

Fig. 1.2 Free vibration with viscous damping

The logarithmic decrement can be experimentally determined from time-history measurements of free vibrations. Normally, two peaks u_1 and u_{n+1} occurring at times t_1 and t_{n+1} and spanning n vibration cycles are considered, in which case we obtain

$$\Lambda = \frac{1}{n} \ln \frac{u_1}{u_{n+1}} \tag{1.1.17}$$

As an example, Fig. 1.2 shows the (calculated) displacement time history for a SDOF system with a natural period of $T_1 = 0.20$ s, an initial velocity at $t = 0$ of 0.6 m/s and a damping value of $D = 5\%$. The positive peak amplitudes of the first four cycles are given as 0.01785, 0.01304, 0.009518, 0.006949 and 0.005071 m, leading to a logarithmic decrement of

$$\Lambda = \ln \frac{0.01785}{0.01304} \approx \frac{1}{4} \ln \frac{0.01785}{0.005071} = 0.315; \quad D \approx \frac{\Lambda}{2\pi} = 0.05 \tag{1.1.18}$$

As mentioned above, the differential equation of motion for the linear SDOF oscillator given by Eq. (1.1.2) with the general initial conditions $u(0) = u_0,\ \dot{u}(0) = \dot{u}_0$ can also be solved by Direct Integration in the time domain. There exist many suitable algorithms for solving this classical initial-value problem.

Two issues are of central importance for the choice of an integration scheme, namely its stability and its accuracy. An unconditionally stable algorithm is present if the solution u(t) remains finite for arbitrary initial conditions and arbitrarily large $\Delta t/T$ ratios, Δt being the time step employed in the integration and T the natural period of the SDOF system, $T = 2\pi\sqrt{m/k}$. A conditionally stable algorithm (which is generally more accurate than an unconditionally stable one) implies that the solution remains finite only if the ratio $\Delta t/T$ does not exceed a certain value. For SDOF systems with known T it is easy to choose a suitable integration time step Δt; however, unconditionally stable algorithms are generally preferable, especially if nonlinearities are to be considered.

The accuracy of a Direct Integration algorithm depends on the loading function f(t), the system's properties and especially on the ratio of the time step Δt to the period T. The deviation of the computed solution from the true one makes itself felt as an elongation of the period and a decay of the amplitude of the former, corresponding to a fictitious additional damping.

Integration algorithms may also be divided into single-step and multi-step methods, which can also be implicit or explicit. Single-step methods, which are quite popular in structural dynamics, furnish the values of u, $\dot{u}$ and $\ddot{u}$ at time $t + \Delta t$ as functions of the same variables at time t alone, while multi-step methods require additional values at times $t - \Delta t$, $t - 2\Delta t$ etc. Multi-step methods therefore involve additional initial computations (e.g. by a single-step algorithm), while single-step methods are "self-starting". Explicit algorithms furnish the solution at time $t + \Delta t$ directly, while in implicit methods the unknowns appear on both sides of algebraic equations and must be determined by solving the corresponding equation system (or just one equation for a SDOF system). This shortcoming of implicit algorithms is offset by their better stability properties.

The well-known NEWMARK β-γ-algorithm, to be used here, is an implicit, single-step scheme with two parameters β and γ which determine its stability and accuracy properties. Considering the time points t_1 and t_2, with $t_2 = t_1 + \Delta t$, the dynamic equilibrium of the SDOF system at time t_2 is given by

$$m\ddot{u}_2 + c\dot{u}_2 + ku_2 = F(t_2) = F_2 \tag{1.1.19}$$

Introducing increments of the displacement, velocity, acceleration and external force according to $\Delta u = u_2 - u_1$, $\Delta\dot{u} = \dot{u}_2 - \dot{u}_1$ etc. leads to the incremental version of Eq. (1.1.2)

$$m\,\Delta\ddot{u} + c\,\Delta\dot{u} + k\,\Delta u = \Delta F \tag{1.1.20}$$

The increments $\Delta\ddot{u}$, $\Delta\dot{u}$ can be given as functions of the displacement increment Δu and the known values of velocity and acceleration at time t_1:

$$\begin{aligned}\Delta\dot{u} &= \frac{\gamma}{\beta\Delta t}\Delta u - \frac{\gamma}{\beta}\dot{u}_1 - \Delta t\left(\frac{\gamma}{2\beta} - 1\right)\ddot{u}_1\\ \Delta\ddot{u} &= \frac{1}{\beta(\Delta t)^2}\Delta u - \frac{1}{\beta\Delta t}\dot{u}_1 - \frac{1}{2\beta}\ddot{u}_1\end{aligned} \tag{1.1.21}$$

Values of $\beta = 1/4$ and $\gamma = 1/2$ correspond to an unconditionally stable scheme which assumes a constant acceleration $\ddot{u}$ between t_1 and t_2. For $\beta = 1/6$ and $\gamma = 1/2$ the integrator is only conditionally stable and the acceleration varies linearly between t_1 and t_2. The displacement increment Δu is given by

$$\Delta u = \frac{f^*}{k^*} \tag{1.1.22}$$

with

$$k^* = m\frac{1}{\beta \Delta t^2} + c\frac{\gamma}{\beta \Delta t} + k \tag{1.1.23}$$

and

$$f^* = \Delta F + m(\frac{\dot{u}_1}{\beta \Delta t} + \frac{\ddot{u}_1}{2\beta}) + c\left(\frac{\gamma \dot{u}_1}{\beta} + \ddot{u}_1 \Delta t(\frac{\gamma}{2\beta} - 1)\right) \tag{1.1.24}$$

The NEWMARK algorithm is used in the programs SDOF1 and SDOF2, details on which can be found in Appendix. The SDOF1 program deals with the case when F(t) is an arbitrary piecewise linear function, while SDOF2 considers steady-state excitations of the type $F(t) = A \cdot \sin(\Omega_1 t) + B \cos(\Omega_2 t)$. For SDOF1 it is usually necessary to first use the program LININT, also described in Appendix, for determining additional values of the forcing function F(t) for the chosen time step Δt by linear interpolation.

Example 1.1
The task is to determine the maximum displacement u of the girder and also the maximum bending moment at the base of the central column for the frame shown in Fig. 1.3. Further data: Mass m = 12 t (assumed to be concentrated in the girder), damping value D = 1%, bending stiffness values $EI_G = 1.25 \times 10^5$ kNm^2, $EI_1 = 0.75 \times 10^5$ kNm^2, all beams and columns are considered to be inextensional ($EA \to \infty$).

The single-story two-bay frame can be modelled using a SDOF idealization as depicted in Fig. 1.1, with mass m = 12 t and spring stiffness k in kN/m. The latter can be determined from statics as the reciprocal of the horizontal girder displacement u due to a unit force F = 1.0 kN (program FRAME) or by carrying out a static condensation for the horizontal girder displacement as a master DOF (program CONDEN, see Sect. 1.2.1). Here, the first approach will be used based on the discretization

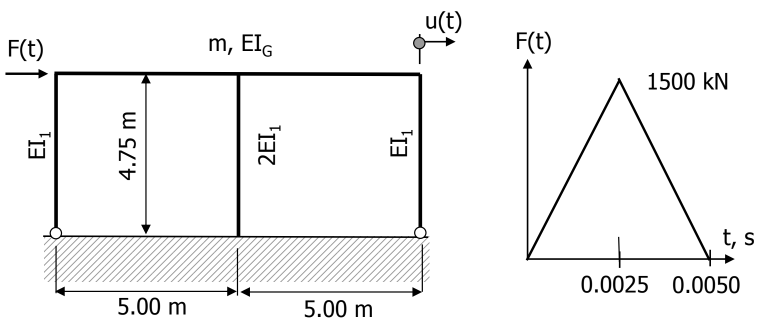

Fig. 1.3 Plane frame with triangular loading function F(t)

<table>
<tr><th>Discretized system</th><th>Input file EFRAM.txt</th></tr>
<tr><td>

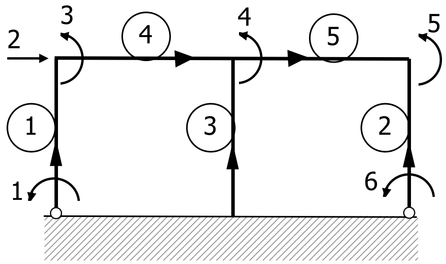

</td><td>

```
75000.,  4.75, 0., 90.
75000.,  4.75, 0., 90.
150000., 4.75, 0., 90.
125000., 5.0, 0., 0.
125000., 5.0, 0., 0.
0,0,1, 2,0,3,
0,0,6, 2,0,5,
0,0,0, 2,0,4,
2,0,3, 2,0,4,
2,0,4, 2,0,5,
0.,1.0, 0., 0., 0., 0.
```

</td></tr>
</table>

Fig. 1.4 Discretization and input file for a unit load at DOF no. 2

of Fig. 1.4 (see input description for the program FRAME in Appendix), using the 6-DOF beam element shown in Fig. 1.46. For more details on the use of the program FRAME and the matrix deformation method of analysis employed here see Example 1.5.

The program FRAME yields a horizontal displacement of the girder due to the unit load (1 kN) equal to 6.292×10^{-5} m. The reciprocal is the spring stiffness, which in this case equals $k = 15{,}893$ kN/m. With k and m known, the undamped circular natural frequency of the frame is

$$\omega_1 = \sqrt{\frac{k}{m}} = \sqrt{\frac{15{,}893}{12}} = 36.39\,\frac{\text{rad}}{\text{s}} \tag{1.1.25}$$

the corresponding natural period being equal to

$$T_1 = \frac{2\pi}{\omega_1} = 0.173\,\text{s} \tag{1.1.26}$$

In view of the characteristics of the load function, a time step Δt of 0.5×10^{-3} s is chosen and the program LININT used to create the file RHS.txt as input file for the program SDOF1. For 600 time points (from zero to 0.3 s) Fig. 1.5 shows the computed time history for the horizontal displacement of the girder (solid line). The maximum displacement is reached at time $t = 0.046$ s and is equal to 0.008445 m or 8.4 mm. In view of the short duration of the excitation, a simple check on the validity of this result can be carried out by using the principle of impulse and momentum, which states that the final momentum of a mass m may be obtained by adding its initial momentum (which, in this case, is zero) to the time integral of the force during the interval considered. This allows the velocity at time $t = 0.005$ s to be determined as follows:

$$m \cdot \dot{u}_1 + \int_0^{0.005} F(t)dt = m \cdot \dot{u}_2$$

$$\rightarrow \dot{u}(0.005) = \frac{\frac{1}{2}1500 \cdot 0.005\,\text{kN s}}{12\,t} = 0.3125\frac{m}{s} \tag{1.1.27}$$

Equation (1.1.11) yields the following expression for the displacement u(t):

$$u(t) = e^{-0.01 \cdot 36.39 \cdot t}\frac{0.3125}{36.39\sqrt{1-0.01^2}}\sin\sqrt{1-0.01^2} \cdot 36.39 \cdot t \tag{1.1.28}$$

This function, depicted as a dashed line in Fig. 1.5, is in almost perfect agreement with the solution obtained using Direct Integration (solid line). From the maximum displacement $u_{max} = 0.00845$ m at $t = 0.046$ s the maximum restoring force is determined as $F_{R,max} = u_{max} \cdot k = 0.00845 \cdot 15{,}893 = 134$ kN. Using the program FRAME with 134 kN as the load corresponding to DOF no. 2 yields a bending moment at the base of the central column equal to 276 kNm. The bending moment diagram for the entire structure is shown in Fig. 1.6.

For a quick assessment of the maximum response of linear undamped SDOF systems subject to impulsive loading, shock or response spectra are quite useful. They present dynamic magnification factors, defined as ratios of maximum dynamic displacements $u_{dyn,max}$ to their static counterparts u_{stat} as functions of the impulse length ratio t_1/T, that is the duration t_1 of the impulse divided by the natural period of the SDOF system. Figure 1.7 shows shock spectra for three impulsive loading shapes, namely rectangular, trapezoidal and triangular.

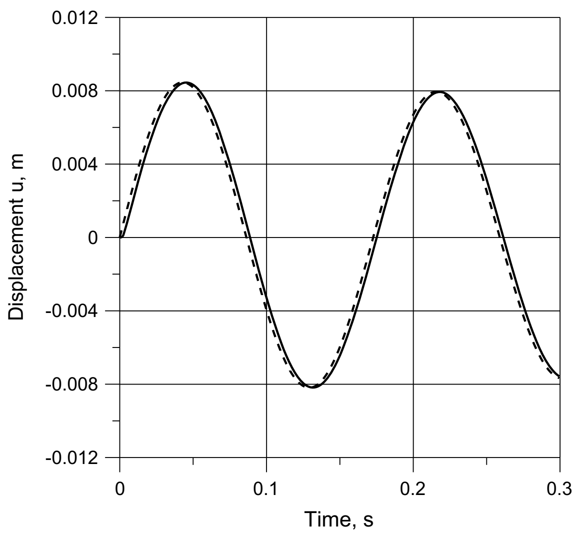

Fig. 1.5 Time histories for the girder horizontal displacement

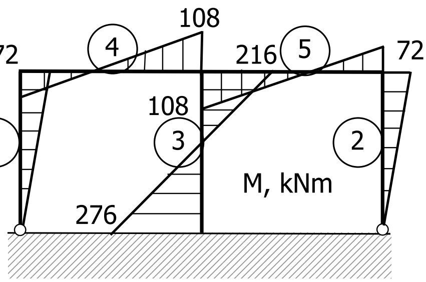

Fig. 1.6 Bending moment diagram at t = 0.00455 s

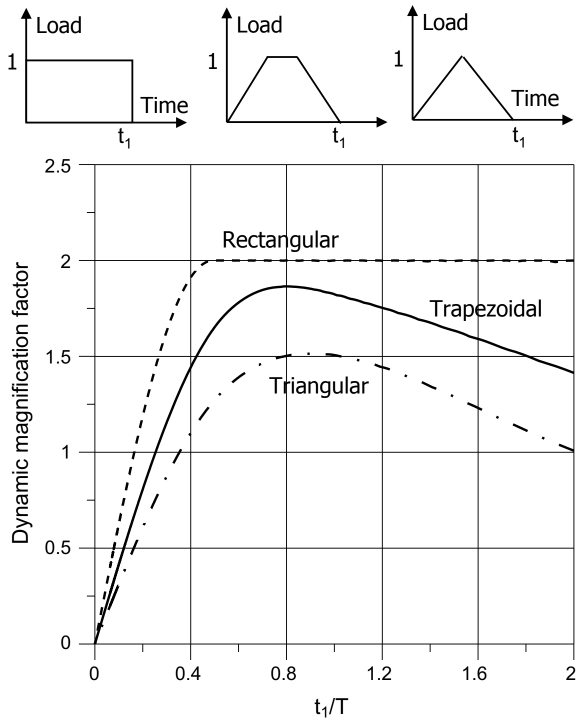

Fig. 1.7 Shock spectra for different impulsive loading shapes

A cursory look at Fig. 1.7 would seem to suggest that dynamic magnification factors do not exceed 2.0, which, however, is not the case. As an example, Figs. 1.8 and 1.9 show some more shock spectra for piecewise linear and sinusoidal impulse shapes. In Fig. 1.8 the solid line corresponds to the positive/negative impulse shown to the left and the dashed line to the positive/positive one shown to the right, while in Fig. 1.9 the solid line corresponds to the single half-sine and the dashed line to the double half-sine impulse.

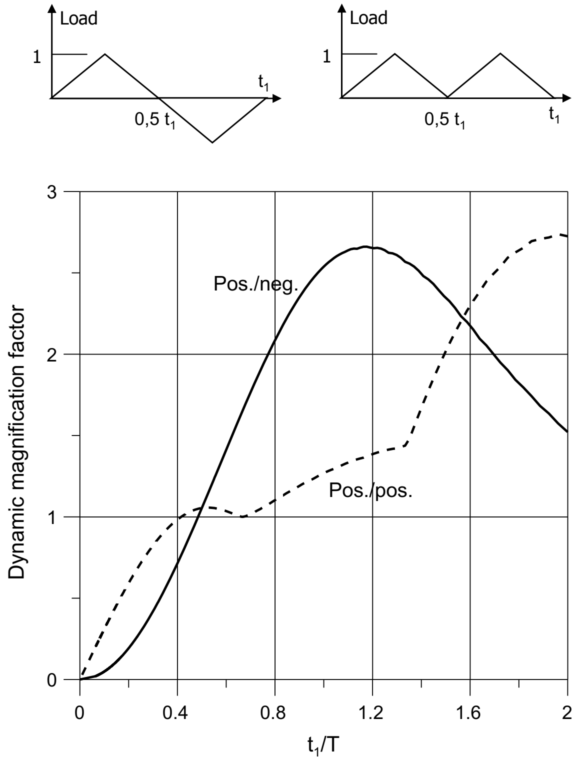

Fig. 1.8 Additional shock spectra for further polygonal impulses

A special case with significant practical importance is the linear SDOF system subject to stationary harmonic excitation as shown schematically in Fig. 1.10.

Its equation of motion is given by

$$\ddot{u} + 2\xi\omega_1\dot{u} + \omega_1^2 u = \frac{F_o}{m}\sin\Omega t \tag{1.1.29}$$

It has the general solution

$$u(t) = \exp(-\xi\omega_1 t)(A\ \sin\omega_D t + B\ \sin\omega_D t) + \frac{F_o}{k}\frac{1}{(1-\beta^2)^2+(2\xi\beta)^2}[(1-\beta^2)\sin\Omega t - 2\xi\beta\cos\Omega t] \tag{1.1.30}$$

where β is the ratio of the excitation frequency to the natural frequency of the system, that is

$$\beta = \frac{\Omega}{\omega_1} \tag{1.1.31}$$

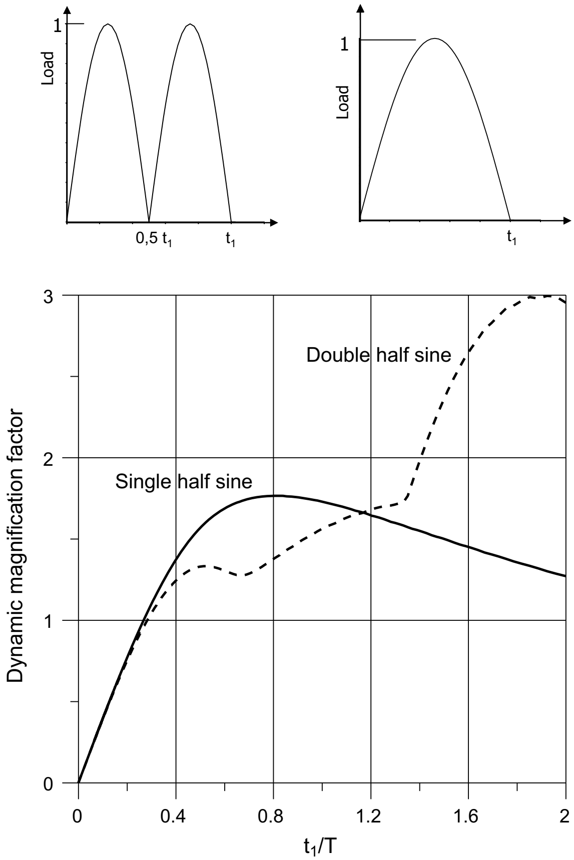

Fig. 1.9 Shock spectra for sinusoidal impulses

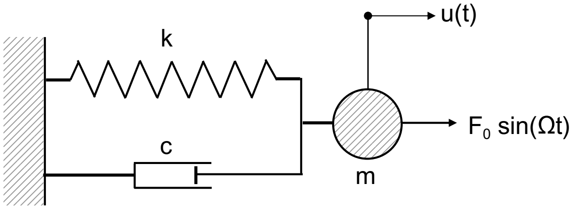

Fig. 1.10 SDOF system under harmonic excitation

The first part of the expression in Eq. (1.1.30) is the solution of the homogeneous differential equation; its constants A and B must be determined from the initial conditions. The second part is the particular integral which depends on the loading; this is the most important part of the system response, since the first part is eventually damped out, as is evident from the factor $e^{-\xi\omega_1 t}$. The second part of the solution can be written down in the form

$$u(t) = u_R \sin(\Omega t - \varphi) \tag{1.1.32}$$

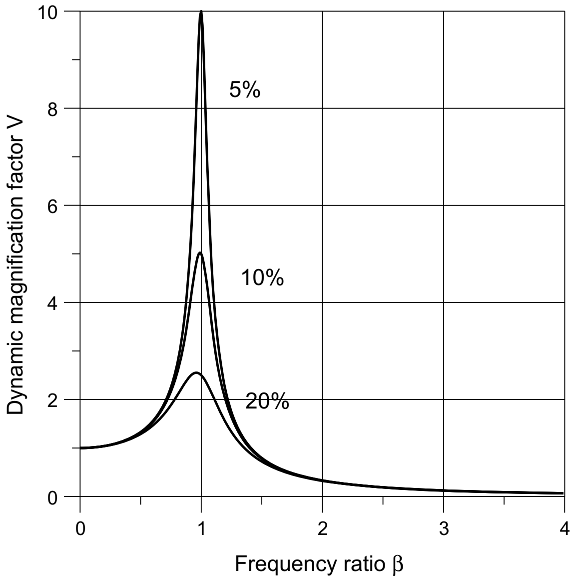

Fig. 1.11 Magnification factor V for different damping ratios D

with

$$u_R = \frac{F_o}{k}[(1-\beta^2)^2 + (2\xi\beta)^2]^{-0.5} \tag{1.1.33}$$

and

$$\varphi = \arctan\frac{2\xi\beta}{1-\beta^2} \tag{1.1.34}$$

From Eq. (1.1.33) the dynamic magnification factor V defined as

$$V = [(1-\beta^2)^2 + (2\xi\beta)^2]^{-0.5} \tag{1.1.35}$$

can be extracted. It is seen to be equal to the ratio of the dynamic to the static response of the harmonically excited SDOF system, where the maximum dynamic response is given by

$$\max u_p(t) = u_R = \frac{F_0}{k}V \tag{1.1.36}$$

Figure 1.11 shows V as a function of the frequency ratio for three damping ratios, namely D = 5, 10 and 20%; clearly, for undamped systems ($\xi = 0$), V tends to infinity.

Peak values of the magnification factor occur at the frequency ratio

$$\beta = \sqrt{1-2\xi^2} \tag{1.1.37}$$

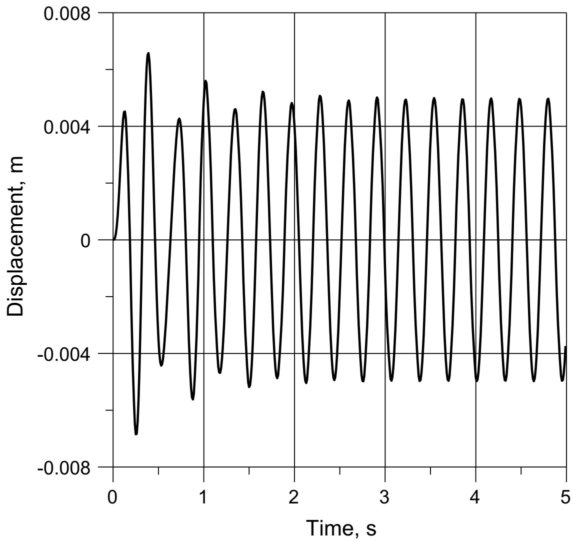

Fig. 1.12 Example 1.2, time history of displacement

They amount to

$$\max\ V = \frac{1}{2}\frac{1}{\xi\sqrt{1-\xi^2}} \tag{1.1.38}$$

For a damping ratio of 1% this gives a peak value of 50, for 5% of about 10 and even for a highly damped system with D = 20% we obtain V = 2.55.

Example 1.2

Consider the system of Fig. 1.10 with the following data: Spring stiffness k = 9000 kN/m, m = 10 t, F_0 = 25 kN, Ω = 20 rad/s and D = 5%. Determine the displacement and velocity time histories u(t) and $\dot{u}(t)$ as well as the maxima of the restoring force and the damping force.

The circular natural frequency ω_1 of the SDOF system is equal to $\sqrt{\frac{k}{m}} = \sqrt{\frac{9000}{10}} = 30\ \frac{\text{rad}}{\text{s}}$, corresponding to $T_1 = 0.21$ s. The program SDOF2 produces the results shown for the time histories of the displacement (Fig. 1.12) and the velocity (Fig. 1.13) using a time step of 0.005 s. The maximum restoring force F_R occurs at time 0.25 s, corresponding to a maximum displacement of −0.00688 m, and is equal to $k \cdot u_{max} = -61.9$ kN, while the maximum velocity of 0.161 m/s, occurring at t = 0.32 s, produces a damping force equal to

$$2 \cdot \xi \cdot \omega_1 \cdot m \cdot \dot{u} = 2 \cdot 0,05 \cdot 30 \cdot 10 \cdot 0.161 = 4.83\,\text{kN} \tag{1.1.39}$$

Both these values were reached during the initial vibration stage, before the viscous damping mechanism eliminated the contribution of the “homogeneous” part

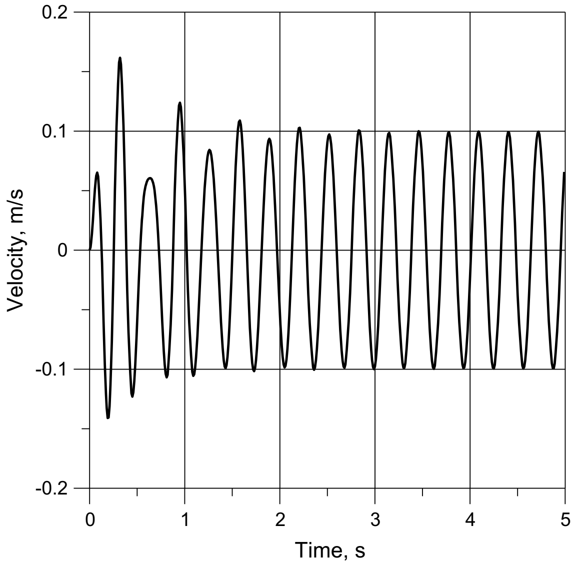

Fig. 1.13 Example 1.2, time history of velocity

of the solution. In the subsequent steady-state harmonic vibration stage, with a frequency ratio of

$$\beta = \frac{\Omega}{\omega_1} = \frac{20}{30} = 0.667 \tag{1.1.40}$$

the maximum displacement amounts to

$$\max u_p(t) = \frac{F_0}{k} V = \frac{25}{9000} V(0.667) = \frac{25}{9000} 1.79 = 0.005\,\text{m} \tag{1.1.41}$$

Since here u(t) is a sine wave with circular frequency Ω, the maximum velocity is readily determined as

$$\max \dot{u} = \Omega \cdot u_{max} = 20 \cdot 0.005 = 0.1\,\text{m/s} \tag{1.1.42}$$

1.1.2 Linear SDOF Systems in the Frequency Domain

It can be shown that any real periodic function of time with period T

$$f(t + T) = f(t) \tag{1.1.43}$$

can be expressed in the form

$$f(t) = a_0 + \sum_{k=1}^{\infty} a_k \cos \omega_k t + \sum_{k=1}^{\infty} b_k \sin \omega_k t \qquad (1.1.44)$$

with the coefficients

$$a_0 = \frac{\omega}{2\pi} \int_0^{\frac{2\pi}{\omega}} f(t)dt = \frac{1}{T} \int_0^T f(t)\, dt \qquad (1.1.45)$$

and

$$a_k = \frac{2}{T} \int_{-T/2}^{T/2} f(t) \cos \omega_k t\, dt \qquad (1.1.46)$$

$$b_k = \frac{2}{T} \int_{-T/2}^{T/2} f(t) \sin \omega_k t\, dt \qquad (1.1.47)$$

Here, $\omega_k = k\frac{2\pi}{T}$, $k = 1, 2, \ldots\infty$. The coefficients a_k and b_k can be regarded as the real and imaginary part, respectively, of the harmonic component associated with the circular frequency ω_k. They can be displayed along a frequency axis at discrete points ω_k with an increment in rad/s equal to

$$\Delta\omega = \frac{2\pi}{T}; \quad \frac{2}{T} = \frac{\Delta\omega}{\pi} \qquad (1.1.48)$$

Figure 1.14 shows such "comb spectra" consisting of discrete values of the coefficients a_k and b_k every $(2\pi/T)$ rad/s.

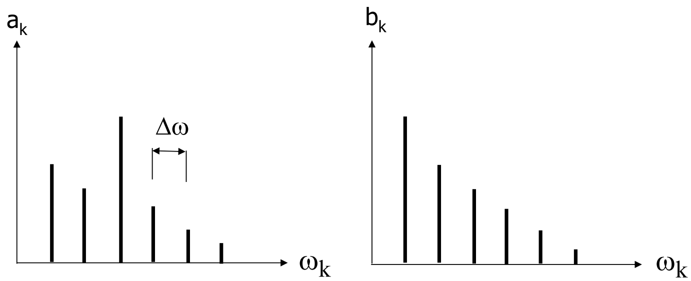

Fig. 1.14 "Comb spectra" for periodic functions

For $a_0 = 0$ we obtain

$$f(t) = \sum_{k=1}^{\infty} \left(\frac{2}{T} \int_{-T/2}^{T/2} f(t) \cdot \cos \omega_k t dt \right) \cos \omega_k t + \sum_{k=1}^{\infty} \left(\frac{2}{T} \int_{-T/2}^{T/2} f(t) \cdot \sin \omega_k t dt \right) \sin \omega_k t \tag{1.1.49}$$

or, using Eq. (1.1.44)

$$f(t) = \sum_{k=1}^{\infty} \left(\frac{\Delta\omega}{\pi} \int_{-T/2}^{T/2} f(t) \cdot \cos \omega_k t dt \right) \cos \omega_k t + \sum_{k=1}^{\infty} \left(\frac{\Delta\omega}{\pi} \int_{-T/2}^{T/2} f(t) \cdot \sin \omega_k t dt \right) \sin \omega_k t \tag{1.1.50}$$

For an aperiodic function we can assume $T \to \infty$, $\Delta\omega \to d\omega$ and

$$f(t) = \int_{\omega=0}^{\infty} \frac{1}{\pi} \left(\int_{-\infty}^{+\infty} f(t) \cdot \cos \omega t\, dt \right) \cdot \cos \omega t\, d\omega + \int_{\omega=0}^{\infty} \frac{1}{\pi} \left(\int_{-\infty}^{+\infty} f(t) \cdot \sin \omega t\, dt \right) \cdot \sin \omega t\, d\omega \tag{1.1.51}$$

Introducing

$$A(\omega) = \frac{1}{2\pi} \int_{-\infty}^{\infty} f(t) \cos \omega t\, dt, \quad B(\omega) = \frac{1}{2\pi} \int_{-\infty}^{\infty} f(t) \sin \omega t\, dt \tag{1.1.52}$$

leads to

$$f(t) = 2 \int_{\omega=0}^{\infty} A(\omega) \cdot \cos \omega t\, d\omega + 2 \int_{\omega=0}^{\infty} B(\omega) \cdot \sin \omega t\, d\omega \tag{1.1.53}$$

and, considering that

$$\begin{aligned} A(\omega) \cdot \cos \omega t &= A(-\omega) \cdot \cos(-\omega t) \\ B(\omega) \cdot \sin \omega t &= B(-\omega) \cdot \sin(-\omega t) \end{aligned} \tag{1.1.54}$$

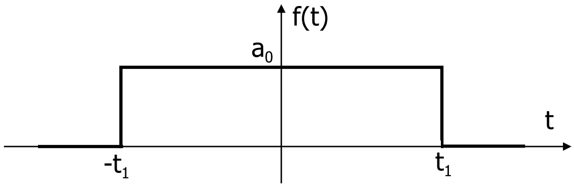

Fig. 1.15 Time domain function

to

$$f(t) = \int_{-\infty}^{\infty} A(\omega) \cdot \cos \omega t \, d\omega + \int_{-\infty}^{\infty} B(\omega) \cdot \sin \omega t \, d\omega \tag{1.1.55}$$

With complex coefficients

$$F(\omega) = A(\omega) - i \cdot B(\omega) \tag{1.1.56}$$

we finally obtain

$$F(\omega) = \frac{1}{2\pi}\left(\int_{-\infty}^{\infty} f(t) \cos \omega t \; dt\right) - i\frac{1}{2\pi}\left(\int_{-\infty}^{\infty} f(t) \sin \omega t \; dt\right)$$

$$F(\omega) = \frac{1}{2\pi}\left(\int_{-\infty}^{\infty} f(t)[\cos \omega t - i \;\sin \omega t]dt\right) \tag{1.1.57}$$

This is the formal definition of the FOURIER transform $F(\omega)$ of the time domain function $f(t)$:

$$F(\omega) = \frac{1}{2\pi}\int_{-\infty}^{\infty} f(t)e^{-i\omega t}dt \tag{1.1.58}$$

The inverse transform is given by

$$f(t) = \int_{-\infty}^{\infty} F(\omega)e^{i\omega t}d\omega \tag{1.1.59}$$

$F(\omega)$ and $f(t)$ form a "FOURIER transform pair". As a simple practical example for transforming a time domain function into the frequency domain, consider the "boxcar" function shown in Fig. 1.15.

The function is even, $f(t) = f(-t)$, so that in Eq. (1.1.52) $B(\omega) = 0$. We obtain